RSC Advances

PAPER

View Article Online
View Journal | View Issue

Cite this: *RSC Adv.*, 2020, **10**, 541

Pulse electromagnetic fields enhance the repair of rabbit articular cartilage defects with magnetic nano-hydrogel†

Jianghong Huang, ‡*[ab] Zhaofeng Jia,‡[c] Yujie Liang,[d] Zhiwang Huang,[e] Zhibin Rong,[f] Jianyi Xiong*[ab] and Daping Wang*[ab]

Hydrogel is an important scaffold material in regenerative medicine and cartilage tissue engineering. Hydrogel material combined with pulse electromagnetic fields (PEMFs), PEMFs has the potential to manage the repair of defective articular cartilage. Here, we developed a new type of magnetic hydrogel. The data shows that the magnetic hydrogel had good mechanical properties, and its surface had micropores and unevenness, which was conducive to cell adhesion growth. Infrared spectroscopy analysis showed that the magnetic particles were evenly distributed in the hydrogel, and the addition of constant static magnetic field yielded magnetic water. The hydrogel exhibited good superparamagnetism. The co-culture of the magnetic hydrogel and bone marrow mesenchymal stem cells (BMSCs) showed good biocompatibility. The PEMFs promoted the differentiation of the BMSCs into cartilage, and the index of cartilage differentiation increased obviously. The results of the animal experiments showed that the magnetic hydrogel and BMSCs combined with pulsed electromagnetic field had a strong repair effect. They also showed that the magnetic nano-hydrogel combined with the PEMFs induced chondrogenic differentiation of the BMSCs. The positive experimental results suggested that the combination of magnetic hydrogel and the PEMFs can be used as an effective method for repairing articular cartilage defects in rabbit model.

Received 27th September 2019
Accepted 18th December 2019

DOI: 10.1039/c9ra07874f

rsc.li/rsc-advances

1. Introduction

Articular cartilage defects, one of the most common orthopedic diseases, pose a major problem in clinical treatment. Due to the limited ability of articular cartilage to repair itself, cartilage replacement is required after injury or lesions. The emergence of tissue-engineered cartilage has brought hope to patients with the condition, and scaffold material plays a crucial role in constructing tissue-engineered cartilage. It not only temporarily replaces or repairs tissue but also provides a growth environment for seed cells. The phenotype of cells will show efficient effects if mechanical stimulation or chemical composition promote cell proliferation, differentiation, and maintenance.[1–4] PEMFs have also been shown to play a crucial role in regulating stem cell proliferation and differentiation. It is well known pulsed electromagnetic field as one kind of mechanical stimulation could promotes proliferation and osteogenic differentiation of human bone marrow stem cells, human adipose-derived stem cells, we have also found that a low frequency pulsed electromagnetic field (PEMFs) could promotes chondrogenic differentiation of MSCs, which could somewhat explain that PEMFs have been widely used in orthopedics.[5–8]

Magnetic nanoparticles (Fe_3O_4) can promote the proliferation and differentiation of mesenchymal stem cells. Magnetic nanoparticles have been found to integrate into the structure of porous scaffolds, and the resulting magnetic scaffold has been found to enhance the proliferation and adhesion of mesenchymal stem cells (MSCs) *in vitro*.[9] Chen *et al.*[10] implanted iron oxide fibrin composite hydrogel prepared by superparamagnetic iron oxide particles into a rabbit cartilage defect model. Combine the chemical composed material with electromagnetic field could render the Electromagnetic chemical effect.[11,12] The magnetic

[a]*Shenzhen National Key Department of Orthopedics, Shenzhen Second People's Hospital, The First Hospital Affiliated to Shenzhen University, Shenzhen 518035, P. R. China. E-mail: huangjianghong88@sohu.com; jianyixiong@126.com; dapingwang1963@qq.com*

[b]*Shenzhen Key Laboratory of Tissue Engineering, Shenzhen Laboratory of Digital Orthopedic Engineering, Shenzhen Second People's Hospital, The First Hospital Affiliated to Shenzhen University, Shenzhen 518035, P. R. China*

[c]*Department of Orthopaedics, Shenzhen People's Hospital, The Second Clinical Medical College of Jinan University, The First Affiliated Hospital of Southern University of Science and Technology, Shenzhen, Guangdong, 518020, P. R. China*

[d]*Shenzhen Kangning Hospital, Shenzhen Mental Health Center, Shenzhen, Guangdong Province, P. R. China*

[e]*Department of Clinical Medicine, Shantou University Medical College, Shantou, Guangdong Province, P. R. China*

[f]*Shijiazhuang Maternal and Child Health Hospital, Shijiazhuang, Hebei Province, P. R. China*

† Electronic supplementary information (ESI) available: Methods and materials. Fig. S1–S4. Tables S1 and S2. See DOI: 10.1039/c9ra07874f

‡ Jianghong Huang and Zhaofeng Jia contributed equally to the work.

nanoparticles (MNPs) and magnetic fields are being combined to enhance osteogenic efficacy.[13,14] The magnetic hydrogel with magnetic fields and stem cells proved enhance chondrogenesis in our previous *in vitro* research.[15]

In the study, we use the magnetically field is designed to produce mechanical stimuli to MSCs, for promoting chondrogenic differentiation. Gelatin, β-cyclodextrin (β-CD), and magnetic nanoparticles (Fe_3O_4) were incorporated to form magnetic nanocomposite hydrogel as internal respond material. Our results show the maximized mechanical stimuli to MSCs, when complex with magnetic nanocomposite hydrogel. They show enhanced chondrogenic differentiation and promoted cartilage repair under magnetic field. This work therefore provides a new type of magnetic tissue-engineered cartilage and promising strategy for implementing magnetic stimuli to help the repair of rabbit knee articular cartilage defects.

2. Experimental

2.1 Reagents and apparatus

Gelatin, β-CD, Fe_3O_4 were purchased from Xincheng Biotechnology Co., Ltd (Shenzhen, China). CCK-8 Cell Proliferation Assay Kit was purchased from Beyotime Co., Ltd. (Shanghai, China). DAPI, 4′,6-diamidino-2-phenylindole dihydrochloride, and Alexa Fluor™ 555 were purchased from Invitrogen (Massachusetts, USA). The primary antibody of COL II was purchased from Abcam (Cambridge, UK). Dulbecco's modified Eagle's high glucose medium, fetal bovine serum, and trypsin were purchased from Thermo Fisher Scientific (USA). MesenGro, supplement, and basic fibroblast growth factor (bFGF) was obtained from the StemRD (California, USA). An alkaline phosphatase detection kit and a Coomassie brilliant blue protein assay kit were purchased from the Major Biotech (Shanghai, China). Reverse transcriptase was from Takara (Dalin, China). Trizol was provided by the Invitrogen (ThermoFisher, USA). The simultaneous mechanical testing machine CTM4000 and infrared spectrometer were located at Shenzhen Vocational and Technical College, and electron microscope was conducted by MIRA3 TESCAN, at Tsinghua University. The electromagnetic field generator was purchased from GE (Boston, USA), and the inverted phase contrast microscope was purchased from OLYMPUS (Tokyo, Japan).

2.2 Preparation of magnetic hydrogels

Gelatin and β-cyclodextrin were dissolved in 2 mL of ultrapure water. Under constant stirring at 400 rpm at 40 °C, GPTMS was added as a crosslinker and Fe_3O_4 magnetic nanoparticles as embedment. Continuous stirring gives a hydrogelation precursor mixture. The precursor solution was then poured into a mold and freeze-dried to form a hydrogel material. The hydrogel materials were soaked in distilled water for 1 day to remove non-crosslinked monomers prior to use.

2.3 Scanning electron microscopy (SEM) and infrared spectroscopy

The morphology of the hydrogels were characterized using a field-emission scanning electron microscopy (MIRA3 TESCAN). After air-drying at room temperature, the samples were gold coated using an ion sputtering device and observed under the electron microscopy. Infrared spectrometer is an instrument that analyzes the molecular structure and chemical composition by utilizing the absorption characteristics of substances with different wavelengths of infrared radiation. When the sample absorbs infrared radiation of a certain frequency, the vibrational energy level of the molecule changes, and the light of the corresponding frequency in the transmitted light beam is weakened, resulting in a difference in the intensity of the corresponding radiation between the reference optical path and the sample optical path, thereby obtaining the infrared spectrum of the measured sample.

2.4 Mechanical, magnetic and rheological tests

Compressive testing of the hydrogels were characterized on a STM Electronic Universal Testing Machine CTM4000. The diameter is set at 10 mm, the thickness at 5 mm, and the loading rate at 5.00 mm min^{-1} (ESI file 1: Fig. S1†). The magnetic hydrogel plus a constant static magnetic field of 100 mT was used for the superparamagnetic function test of the material at a distance of 10 mm between the gel and the magnet. To measure the rheological properties of the hydrogels, the gelation solution was injected onto the surface of the mold or tissue to assess the rate of gelation (ESI file 2: Fig. S2†). A tube tilt method was used to measure the gelation time of the sample, and the test tube containing 2 mL of the gel sample was tilted every 30 s until the sample stopped flowing. For rheology study of flow and deformation of materials, the sample was placed on a rheometer to measure the gelation point of the hydrogel material and the storage moduli G′.

2.5 Cell cultures

The protocol including all the procedures was approved by the animal experimentation and ethics committee of Shenzhen Second People's Hospital. BMSCs from bone marrow were acquired from female New Zealand white rabbit at age of 3 months. Briefly, the rabbit's bone marrow was punctured at the left femur trochanter, and about 3 mL of bone marrow was extracted using a syringe containing 2 mL of heparin. The extracted bone marrow was placed into a 10 mL centrifuge tube, and PBS was added to a final volume of 5 mL. The bone marrow solution was centrifuged at 1200 rpm for 10 min, and the supernatant was discarded. The pellet was washed twice with PBS, followed by centrifugation at 1000 rpm. Then cells were resuspended and grown in MesenGro Medium supplemented with 10% fetal bovine serum (FBS) and 1% penicillin–streptomycin and 10% MesenGro Supplement and 10 ng mL^{-1} of basic fibroblast growth factor (bFGF) in a CO_2 incubator containing 5% CO_2 at 37 °C. After being incubated for three days, the BMSCs of passage 3 were used for further experiments (ESI file 3: Fig. S3†). For chondrogenic differentiation experiment we used serum-free chondrogenic medium, which consisted of DMEM (4.5 g L^{-1} glucose), 1% ITS supplement, 100 nM dexamethasone, 0.17 mM L-ascorbic acid-2-phosphate, 1 mM sodium pyruvate, 0.35 mM L-proline. The chondrogenic

induction medium used here contains 10 ng mL^{-1} TGF-β1, 40 mg mL^{-1} proline, 0.1 mM dexamethasone, 50 mg mL^{-1} ascorbate and 1% Insulin-Transferrin-Selenium Supplement obtained from Cyagen Biosciences (California, USA).

2.6 Cell proliferation assay

The proliferation of the BMSCs grown on the different materials was determined by cell counting kit-8 CCK-8 (purchased from Beyotime, Shanghai, China). BMSCs of 3 × 103 in 200 μL suspension were seeded in various hydrogel materials in 96-well plates and incubated for 1, 3, 5, 7 days in DMEM containing 10% FBS. As a control group, BMSCs of the same density were seeded on 96-wells only. After incubation, cells were collected, rinsed in Hank's salt solution, and then incubated with 100 μL fresh DMEM containing 10% CCK-8 solution and 10% FBS at 37 °C in a 5% CO_2 humidified incubator at 37 °C for 4 h. ODs at 450 nm were measured using a thermo-plate microplate reader (Rayto Life and Analytical Science Co. Ltd, Germany). Error bars represent SDs of the means of three independent experiments.

2.7 Live/Dead viability assay

The viability of cells seeded onto the hydrogels was evaluated by Live/Dead Cell Staining Kit purchased from Tianjin Wei Kai Biological Engineering Co., Ltd. (Tianjin, China), and performed according to the manufacturer's instructions. Briefly, 1 mm thick discs of hydrogels were cut to be fit in the 24-well cell culture plate. The discs were soaked in 75% ethanol overnight for sterilization and then washed by PBS for three times. The sterilized samples were immersed in the culture medium for 24 h. The medium was subsequently removed, and the cells prepared above were seeded onto the hydrogels and incubated at 37 °C with a concentration of 5 × 104 cells per sample. The seeded cell and hydrogel materials were treated with or without PEMFs. After a 7 day incubation, the samples were incubated in 400 μL culture medium with 2 μM calcein-AM (staining live cells) and 4 μM ethidium homodimer-1 (staining for dead cells) for 45 min, then examined under a Leica DM16000B microscope. Images were captured using a Leica DFC550 digital camera and analyzed using a Leica LAS V4.6 software.

2.8 Reverse transcription and real time PCR

Total RNA from BMSCs were extracted using TRIzol reagent following the manufacturer's instructions (Thermo Fisher). The total RNA preparation was reverse transcribed to cDNA using an RT-PCR system for first-strand cDNA synthesis (Takara, China). Real-time PCR was carried out for 40 cycles of amplification: 95 °C for 15 s and 60 °C for the 60 s using SYBR Premix EX Taq (Takara, China) and the gene expression level of COL2, Aggrecan and COL1 was examined on Stratagene Real-Time PCR system (Applied Biosystems, Grand Island, NY, USA). GAPDH was used as an internal control for quantification and relative gene expression was calculated using the $2^{-\Delta\Delta C_T}$ equation. Each sample was analyzed in triplicate. Primer sequences are listed in Table 1.

2.9 Establishment of cartilage defects

Rabbits were placed in a dorsal-recumbent position after general anesthesia induced by injecting 3% pentobarbital sodium into the marginal ear vein at a dose of 1 mL kg^{-1}. The hair on the knee area was shaved and the surgical site was disinfected with the povidone iodine solution and 75% ethanol three times. The rabbits' knee joints were operated on using a medial parapatellar approach. A cylindrical full-thickness cartilage defect (3.5 mm in diameter and 1.5 mm in depth) was created on the trochlear groove using a special drill (ESI file 4: Fig. S4†). Then, the joint capsular was sutured and closed layer by layer using absorbable surgical sutures (VICRYL Plus). After surgery, the rabbits were allowed free movement in their cages. The surgical site was disinfected with 0.1% povidone iodine twice a day for 3 days. Wound healing was monitored for 1 week and no infection was observed. The experiment was divided into four groups, Group (a): magnetic gelatin/β-CD/Fe_3O_4 hydrogel complexed with BMSCs (plus pulsed electromagnetic field), Group (b): magnetic gelatin/β-CD/Fe_3O_4 hydrogel and BMSCs complex, Group (c): magnetic gelatin/β-CD/Fe_3O_4 hydrogel, Group (d): blank control.

2.10 Macroscopic score and histological evaluation of cartilage repair

After 8 and 12 weeks of implantation of specimens at joint defects, all rabbits were sacrificed and the operated distal femur condyles were harvested. The specimens were fixed with 10% formalin solution (Sigma-Aldrich, USA) for 24 h and then decalcified for 24 h with a 10% aqueous solution of nitric acid for paraffin embedding (Sigma-Aldrich, USA). All specimens were cut into sections of 4 μm thickness and stained with hematoxylin–eosin, toluidine blue for morphological analysis. The gross appearance and histological evaluation of the defect sites were photographed and blindly scored by 3 independent observers based on the International Cartilage Repair Society (ICRS) macroscopic scoring system (ESI file 4: Table S1†) and ICRS Visual Histological Assessment Scale (ESI file 5: Table S2†).[16–18]

2.11 Statistical analysis

Data were expressed as means ± standard error of the mean. A statistical difference was performed by Student's *t*-test using the GraphPad Prism version 6.01 Software (GraphPad Software, San Diego, CA). A value of $p < 0.05$ was considered statistically significant.

3. Results

3.1 Synthesis and characterize the magnetic nano-hydrogel

The gelatin, β-CD, and magnetic nanoparticles (Fe_3O_4) were prepared by chemical synthesis and freeze-dried to prepare a novel magnetic nano-hydrogel. At the same time, an ordinary gelatin/β-CD hydrogel was prepared as a control group (Fig. 1A and B). Scanning electron microscopy (SEM) reveal that the surface of the magnetic gelatin/β-CD/Fe_3O_4 hydrogel was uneven, formed rough protrusions, and some large and small

Table 1 Primers designed for the real-time PCR analysis of several chondrogenic differentiation-related genes

Gene symbol	Sequence (5′-3′)	GeneBank accession no.
COL2	CCTGTGCGACGACATAATCTGT GGTCCTTTAGGTCCTACGATATCCT	AF027122
Aggrecan	GCTACGGAGACAAGGATGAGTTC CGTAAAAGACCTCACCCTCCAT	L38480
COL1	ATGGATGAGGAAACTGGCAACT GCCATCGACAAGAACAGTGTAAGT	D49399
GAPDH	CGTCTGCCCTATCAACTTTCG CGTTTCTCAGGCTCCCTCT	L23961

pores existed (Fig. 1C and D). However, the surface of the ordinary gelatin/β-CD hydrogels was relatively flat. Therefore, we suppose that the surface of the magnetic gelatin/β-CD/Fe_3O_4 hydrogel will be more suitable for cell adhesion and proliferation. Infrared spectroscopy showed magnetic particles (Fe_3O_4) existed in the supramolecular magnetic hydrogel as it were appeared at the 630° position (Fig. 1E), which indicated that magnetic particles was contained in the magnetic hydrogel.

Then we performance the superparamagnetic functional analysis, mechanical test analysis, and rheological test analysis. The results of the superparamagnetic function test shown the distance of the magnetic field to the magnetic hydrogel was approximately 1 cm^2 and the magnetic field strength was approximately 100 MT (Fig. 2A–D). Fig. 2E showed that the compressive strength of the hydrogels in both groups increased, the compression modulus of the magnetic hydrogel was 2.79 MPa and 2.25 MPa for the ordinary hydrogel. The rheometer test revealed that the gel point occurred at about 200 s, after which the hydrogel gradually solidified and became hard. The maximum and stable balance (Fig. 2F) and the tube tilt method revealed that the gel sample began to slow down after standing for 30 s, after 3 min, the sample stopped flowing (Fig. S2†). Combining the results of two experimental tests, we found that the novel magnetic nanocomposite hydrogel had an injectable function.

When the hydrogel was implanted in the rabbit body, the mechanical properties of the material played an important role in the hydrogel-tissue integration process. Our synthesis magnetic gelatin/β-CD/Fe_3O_4 hydrogel shown a strong superparamagnetic function and suitable compressive strength as the compression modulus of the human normal cartilage was generally between 0.08 MPa and 50 MPa.[19]

3.2 Cytocompatibility study of magnetic hydrogel

To evaluate the cell proliferation CCK-8 assay was performed. There was no significant difference in cell proliferation in the experimental group and the control group ($P > 0.05$). When grown in magnetic hydrogel, it could promote the proliferation of stem cells under the influence of the PEMFs (Fig. 3A).

The results of Live/Dead cell staining showed that there was significant change observed in cell viability between the control

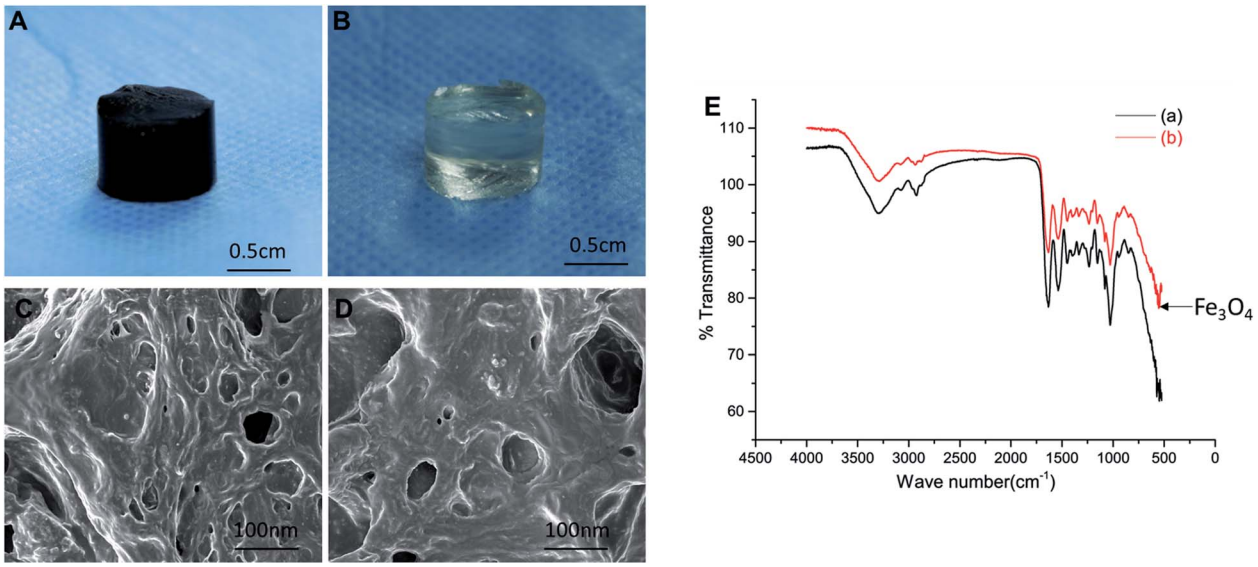

Fig. 1 General view of hydrogel, (A) magnetic gelatin/β-CD/Fe_3O_4 hydrogel, (B) ordinary gelatin/β-CD hydrogel, and (C) SEM of magnetic gelatin/β-CD/Fe_3O_4 hydrogel; the microscopic surface structure is uneven and has micropores. (D) The microscopic surface of the ordinary gelatin/β-CD hydrogel has micropores but is relatively flat. (E) Infrared spectrum: (a) ordinary gelatin/β-CD hydrogel and (b) magnetic gelatin/β-CD/Fe_3O_4 hydrogel.

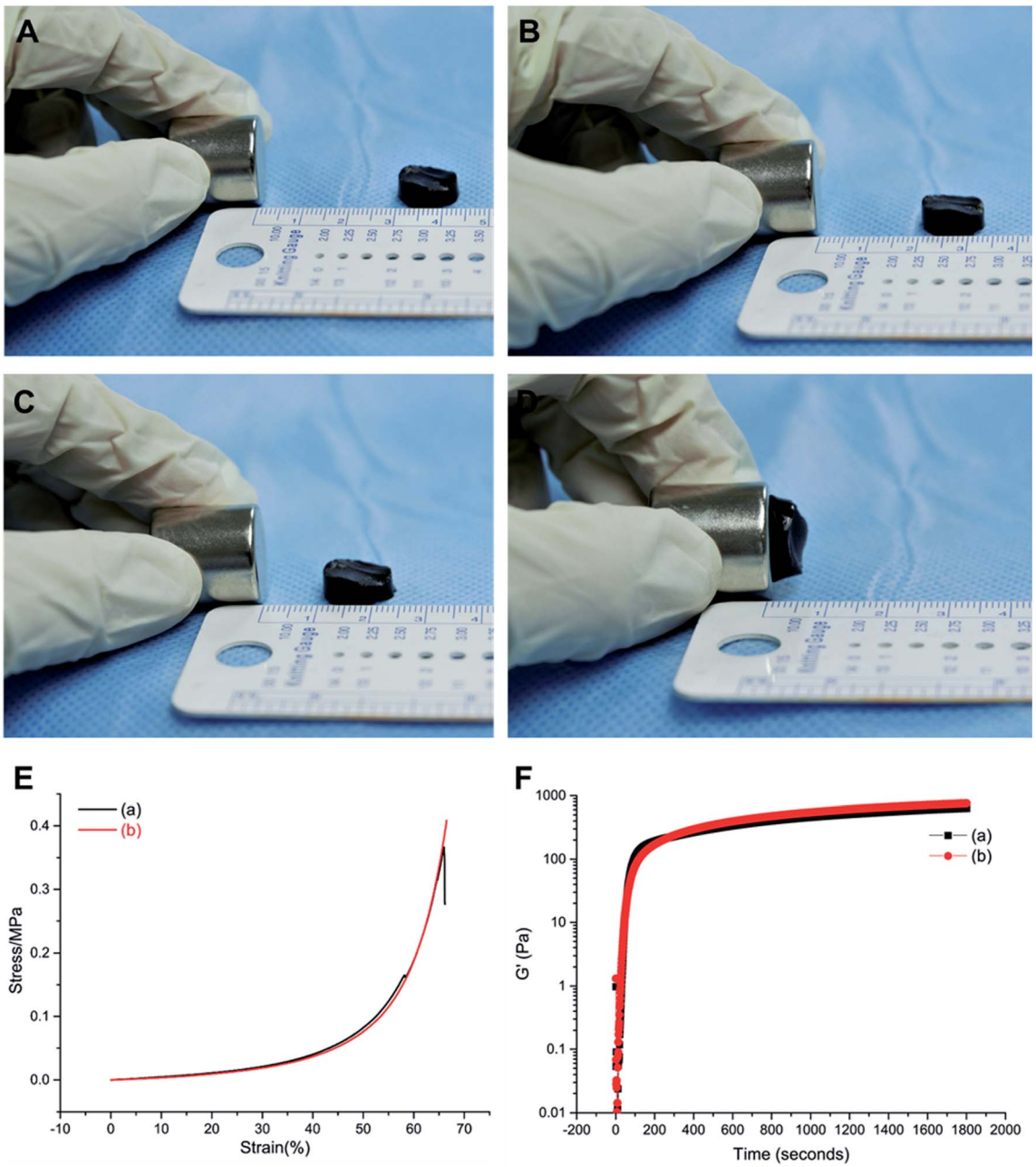

Fig. 2 Characterization of the superparamagnetic properties of the magnetic gelatin/β-CD/Fe_3O_4 hydrogels (A–D), (E) mechanical test results of hydrogel: (a) ordinary gelatin/β-CD hydrogel and (b) magnetic gelatin/β-CD/Fe_3O_4 hydrogel. (F) Hydrogel rheological test results: (a) ordinary gelatin/β-CD hydrogel and (b) magnetic gelatin/β-CD/Fe_3O_4 hydrogel.

group and the experimental group (Fig. 3B). These results demonstrated magnetic hydrogel has good biocompatibility.

3.3 Chondrogenic differentiation potential of PEMFs combined with magnetic hydrogel

The BMSCs seed on the scaffolds with the additional PEMFs, we observed that a significant expression of almost all late chondrogenic differentiation markers. More specifically, there was a pronounced upregulation of *COL2* and *Aggrecan* after 21 days (Fig. 4). During the culture, the PEMFs combined with the magnetic hydrogel significantly enhanced the expression of cartilage-specific gene markers, such as *COL2*, *Aggrecan*, and *COL1*, thereby inducing the differentiation of the BMSCs into chondrocytes. In summary, we demonstrated that PEMFs combined with magnetic nanocomposite hydrogel scaffolds promoted cartilage differentiation.

3.4 Magnetic hydrogel composite stem cells plus PEMFs for cartilage repair

Rabbits were sacrificed at 8 and 12 weeks after the specimens of each group were implanted in the cartilage defect, and the femoral condyles were harvested. We first evaluated the

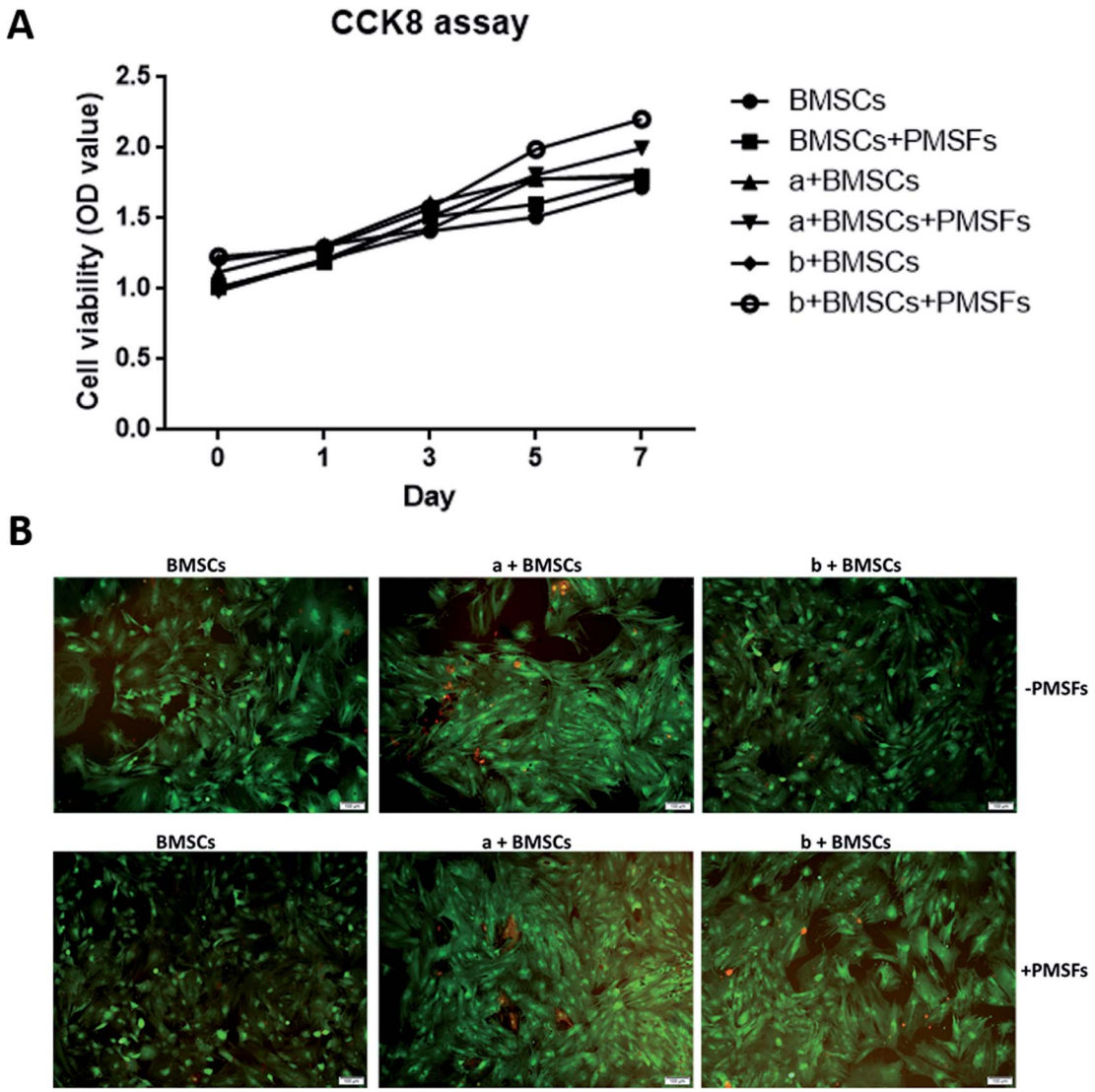

Fig. 3 (A) CCK-8 solution absorption: (a) ordinary gelatin/β-CD hydrogel and (b) magnetic gelatin/β-CD/Fe_3O_4 hydrogel. (B) Live/Dead cell staining: (a) ordinary gelatin/β-CD hydrogel and (b) magnetic gelatin/β-CD/Fe_3O_4 hydrogel.

performance of cartilage repair through rough observation (Fig. 5A–H). After 8 and 12 weeks, Group (d), the blank control group, still had clear boundaries between normal tissues and defects (Fig. 5D and H). Defects in Group (c) were covered by thin layer fibrous tissue at 8 weeks and were completely covered by white hyperproliferative fibrous tissue at 12 weeks (Fig. 5C and G). The regenerated tissue in Group (b) covered approximately 50% of the defects at 8 weeks, whereas the

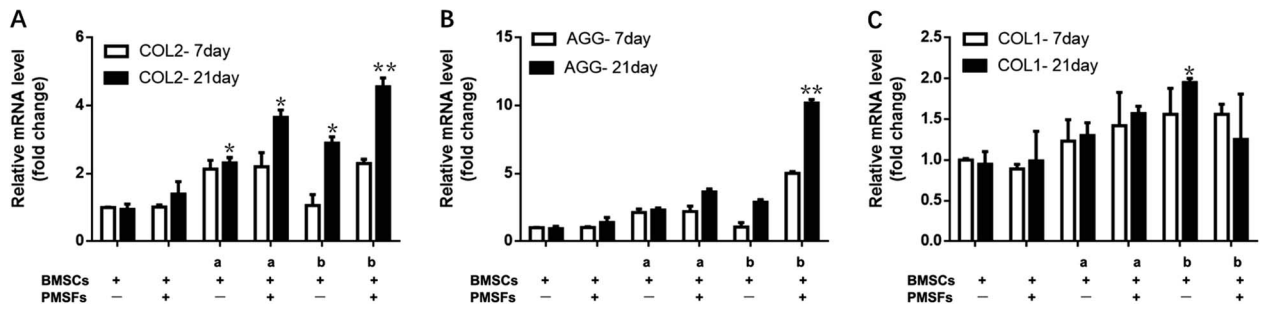

Fig. 4 Real-time PCR analysis of the expression of chondrogenic markers, including (A) COL2, (B) Aggrecan, and (C) COL1 after 7 and 21 days. Values are means of $n = 3$ (± SD). Grouping in the figure: (a) ordinary gelatin/β-CD hydrogel and (b) magnetic gelatin/β-CD/Fe_3O_4 hydrogel.

defects were repaired at around 70% at 12 weeks (Fig. 5B and F). The regenerated tissue in Group (a) covered more than 80% of the defects at 8 weeks, and the defects were completely repaired at 12 weeks (Fig. 5A and E). Therefore, Group (a) showed better repair effects than the other three groups. We used the ICRS macroscore to further evaluate both time points, and both Groups (a) and (b) had much higher scores than the other two groups, which indicated that the magnetic material binding to stem cells had a better effect on cartilage repair (Fig. 5I and J). The score of the applied pulsed electromagnetic field Group (a) was significantly higher than that of the pulsed electromagnetic field Group (b). Therefore, based on general observation, we found that the PEMFs combined with magnetic hydrogels were more conducive to cartilage defect repair.

The histological analyses of repaired cartilage shown cartilage damage in the control Group (d) resulted in significant cavities and fibrous tissue formation after 8 weeks (Fig. 6M and N). The damaged area decreased after 12 weeks and was covered by some inflammatory tissues (Fig. 6O and P). Animals in Group (c) were more effectively repaired than those in Group (d). However, the regenerated tissue was fibrous, and the gap between the new tissue and the natural cartilage was evident at 8 weeks (Fig. 6I and J). After 12 weeks, the regenerated tissue was predominantly hyperproliferative fibrous tissue, while only a small fraction was cartilage-like tissue (Fig. 6K and L). Group (b) was able to regenerate cartilage better, and cartilage tissue partially formed in the defect at 8 weeks (Fig. 6E and F). After 12 weeks, the regenerative tissue had filled 70% of the defects (Fig. 6G and H). Group (a) had the best repair effect, and cartilage tissue was newly formed in the

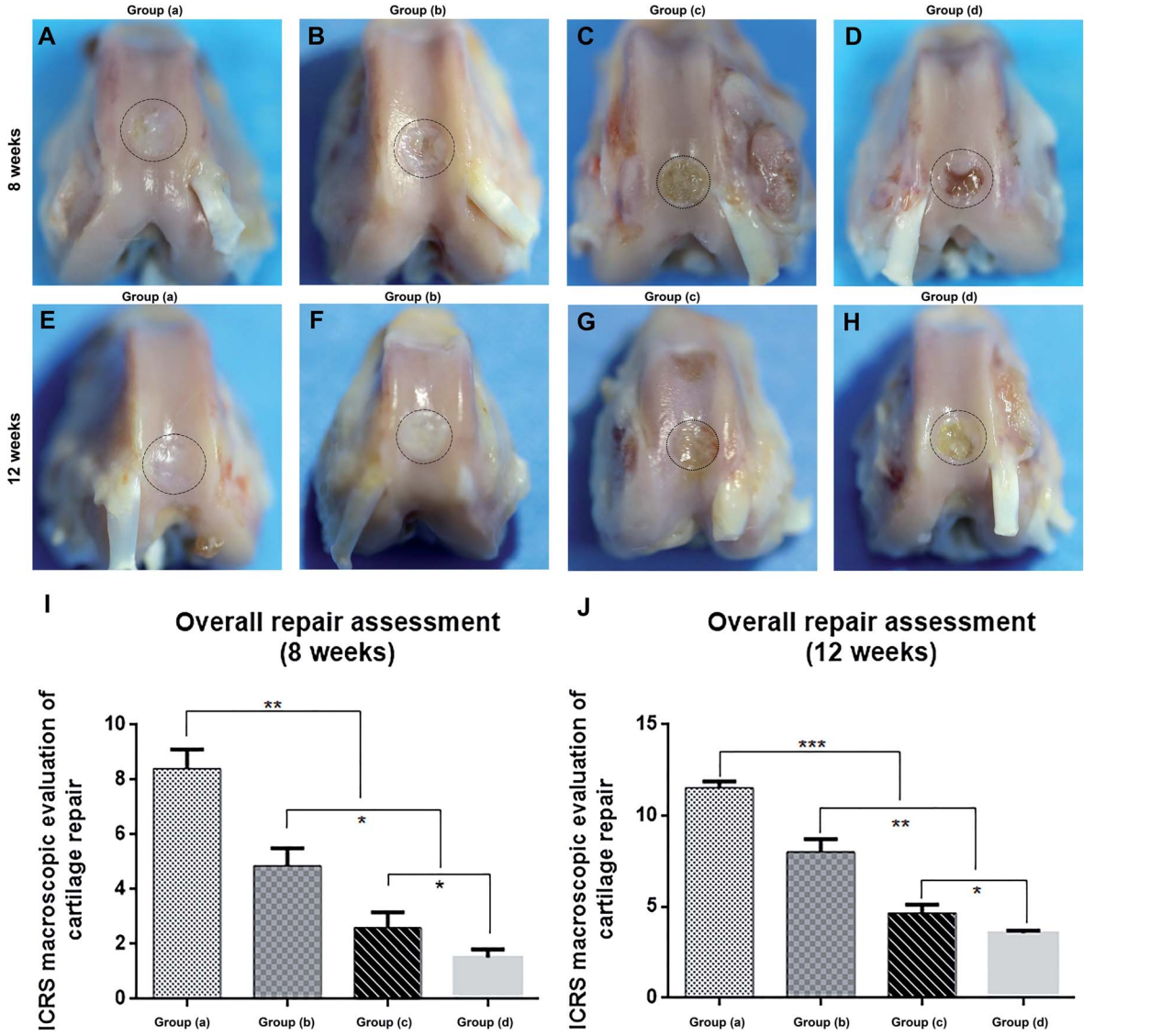

Fig. 5 The macroscopic assessment of repaired articular cartilage. (A–H) Photographs of rabbit knee articular defects at 8 and 12 weeks after operation. The black circles indicate the original defect margin. (I and J) The ICRS macroscopic scores of the repaired cartilage at 8 and 12 weeks. Data are presented as mean ± SD ($n = 6$, $^{*}P < 0.05$, $^{**}P < 0.01$, and $^{***}P < 0.001$). Group (a) magnetic gelatin/β-CD/Fe_3O_4 hydrogel complexed with BMSCs (plus pulsed electromagnetic field), Group (b) magnetic gelatin/β-CD/Fe_3O_4 hydrogel and BMSCs complex, Group (c) magnetic gelatin/β-CD/Fe_3O_4 hydrogel, Group (d): blank control.

defect at 8 weeks (Fig. 6A and B). After 12 weeks, the regenerative tissue had completely filled the defects, which had histological staining similar to that of natural cartilage (Fig. 6C and D).

We further evaluated the repair effect based on the ICRS Visual Histology Assessment Scale System (Fig. 6Q and R). Similar to our other observations, the other three groups of treatment resulted in better repair compared to the blank control group. However, PEMFs combined with magnetic hydrogel repair Group (a) had significantly higher repair scores. Overall, PEMFs combined with magnetic hydrogel repair showed the best effect in Group (a) after the post-injury regeneration of cartilage.

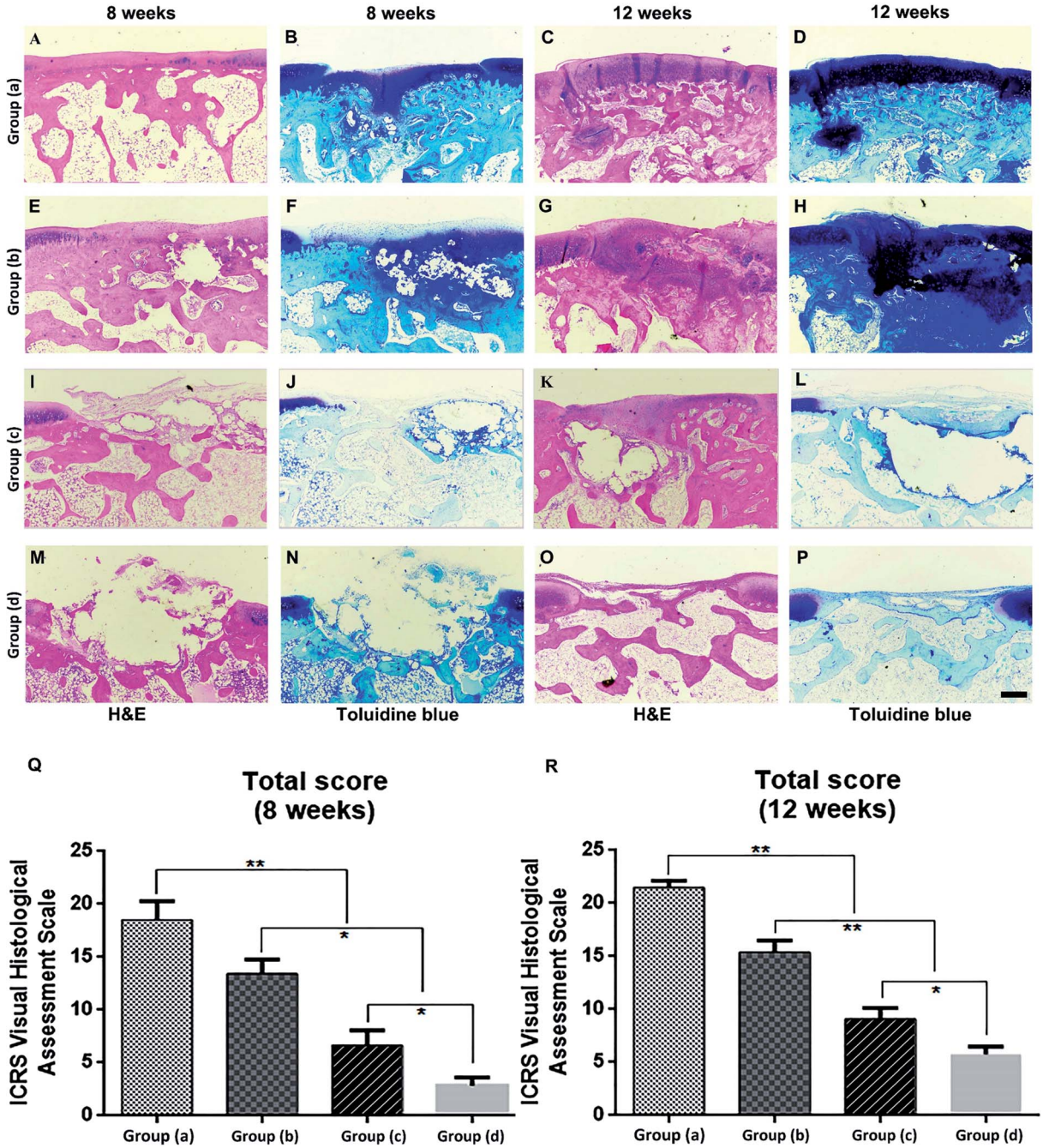

Fig. 6 The histological evaluations of the repaired articular cartilage. (A–P) Representative hematoxylin and eosin and toluidine blue staining of repaired articular cartilage at 8 and 12 weeks after implantation. Scale bar: 500 μm. (Q and R) Assessment by the ICRS Visual Histological Assessment Scale for repaired cartilage at 8 and 12 weeks after implantation. Data are presented as mean ± SD ($n = 6$, *$P < 0.05$, **$P < 0.01$). Group (a) magnetic gelatin/β-CD/Fe_3O_4 hydrogel complexed with BMSCs (plus pulsed electromagnetic field), Group (b) magnetic gelatin/β-CD/Fe_3O_4 hydrogel and BMSCs complex, Group (c) magnetic gelatin/β-CD/Fe_3O_4 hydrogel, Group (d): blank control.

4. Discussion

Due to the limited self-regeneration potential of natural cartilage, articular cartilage tissue repair is, in general, challenging.[20,21] In the past few years, the combination of scaffold and stem cell based tissue engineering technologies has hold great promise repairing complex cartilage defects.[22,23] BMSCs are readily available and highly proliferative, making them ideal sources of cartilage repair.[24,25]

Developing a dual functional scaffold with physical and chemical properties is expected to more efficiency to simultaneously regenerate the cartilage. The magnetic hydrogel is a composite of a hydrogel matrix and a magnetic material. Different hydrogel matrices affect the performance of magnetic hydrogels. Gelatin is a hydrolysate of collagen. It is an important component of the extracellular matrix and has excellent biocompatibility. Moreover, β-cyclodextrin acts as an organic compound. Our result showed good biocompatibility of gelatin/β-cyclodextrin hydrogel as the main matrix component for the preparation of the new magnetic nano-hydrogel. The scaffold material acts as an exogenous cellular vector to promote the movement, adhesion, proliferation, and differentiation of bone marrow mesenchymal stem cells, or to provide structural support. The mechanical test results of the hydrogel in this experiment showed that the magnetic gelatin/β-CD/Fe_3O_4 hydrogel had better mechanical properties and maintained a strong self-healing function after the stress test, which may have been due to the addition of β-CD and Fe_3O_4 in gelatin. β-CD plays a role in enhancing the mechanical properties of the composite hydrogel and also has the viscosity needed to promote the repair of cartilage.

It's well known that magnetic particle materials impart special magnetic properties to magnetic hydrogels and are superparamagnetic.[26,27] This means that they respond to changes in the magnetic field of the external environment. The magnetic properties of magnetic hydrogels depend to a large extent on the type of magnetic particles, the particle size,[28] and the content.[29] Magnetic nanoparticles also have the ability to bind to the cell surface, and the response of magnetic particles under the influence of external magnetic fields makes it possible to influence cell differentiation and proliferation.[30–32] But we think that the benefit effect of magnetic stem cell phenotype needs further external stimulation. By applying external magnetic device, such as PEMFs could stimulate fracture healing and cartilage repair and used as a non-invasive, simple, and side-effect method in the clinical prevention. As described in previous studies, PEMFs promoted the growth and proliferation of mesenchymal stem cells *in vitro*, which caused them to be differentiated into cartilage-like cells.[33,34] The biological effects have certain known correlations with the parameters of PEMFs, but the mechanism of the action remains unclear.

We fabricated a novel magnetic hydrogel scaffold then the viability, proliferation and chondrogenic differentiation in the PEMFs status were assessed *in vitro*.[35,36] After that, we transplanted BMSCs complex with the magnetic hydrogel scaffold into the knee joint defects of New Zealand white rabbits. We then added PEMFs to stimulate repair and evaluated the cartilage repair index. The results of the study showed that after 12 weeks, the magnetic hydrogel and BMSCs combined with the PEMFs completely repaired the knee articular cartilage defects in the rabbits. This proved that the pulsed electromagnetic field had a very good effect on the rabbit cartilage repair after the composite of the magnetic hydrogel and BMSCs. Therefore, we concluded that PEMFs combined with magnetic nanocomposite hydrogels can serve as a reliable method for cartilage tissue engineering. In addition, the study can be used to advance the development of magnetic strategies in tissue engineering to repair damaged cartilage tissue.

This study also had some limitations. The intensity of the pulsed electromagnetic field used for cartilage repair was relatively fixed. It was also uncertain whether the newly regenerated tissue was completely induced by the magnetic hydrogel-complexed BMSCs. Finally, in our animal studies, we observed and evaluated the results after 8 and 12 weeks. This follow-up time may have been too short to yield a more significant difference in the quality of the repair.

5. Conclusion

Researchers in cartilage tissue engineering have been working to develop a cartilage tissue-engineering scaffold material that has sufficient mechanical strength, high biocompatibility, and hydrophilicity and is easily degraded and absorbed. The magnetic nano-hydrogel material prepared in this experimental study exhibited not only the above excellent characteristics but also a superparamagnetic effect and was co-cultured with the magnetic hydrogel under the stimulation of a pulsed electromagnetic field. BMSCs can be proliferated and differentiated into chondrocytes and can bind to the cell surface more closely. The results of the animal experiments also showed that the magnetic gelatin/β-CD/Fe_3O_4 hydrogel combined with BMSCs had a better effect on the knee joint injury repair of rabbits under the stimulation of pulsed electromagnetic field. Based on our results, we predict that a pulsed electromagnetic field combined with magnetic hydrogel would have a good chondrogenic differentiation effect on bone marrow mesenchymal stem cells. Thus, our study is very exciting as it combines tissue engineering and PMSFs approaches to successfully repair defective articular cartilage. The approach should be adaptable in the future to human cartilage tissue engineering treatment.

Ethical statement

The protocol including all the procedures was approved by the animal experimentation and ethics committee of Shenzhen Second People's Hospital and were performed in accordance with the Guidelines for Care and Use of Laboratory Animals of Southern Medical University.

Author contributions

J. H. and Z. J. contributed equally to the work. J. H. and Z. J. performed most of the experiments and wrote the manuscript. Y. L. and Z. H. helped on characterization. Z. R. supported the experiments. J. Xiong and D. W. designed the experiments. All the authors reviewed and commented on the manuscript at all stages.

Conflicts of interest

The authors declare no conflict of interest.

Acknowledgements

The authors acknowledge funding from Guangdong Province Science and Technology Project (Grant No. 2017A020215116), Shenzhen R&D funding Project (JCYJ20160301111338144, JCYJ20170306092315034, JCYJ20160429185235132), Health and Family Planning Commission of Shenzhen Municipality Project (SZXJ2018035). The fund of the young and middle-aged scientific research backbone cultivation project of Shenzhen People's Hospital (No. SYKYPY201903). Fund for High-Level Medical Discipline Construction of Shenzhen University (Grant No. 2016031638). This work was also funded by Science and Technology Innovation Committee of Shenzhen (JCYJ20180306170922163), Sanming Project of Medicine in Shenzhen (No. SZSM201612079).

References

1 Y. Zhou, K. Liang, S. Zhao, C. Zhang, J. Li, H. Yang, X. Liu, X. Yin, D. Chen, W. Xu and P. Xiao, *Int. J. Biol. Macromol.*, 2018, **108**, 383–390.
2 H. Ghuman, M. Gerwig, F. J. Nicholls, J. R. Liu, J. Donnelly, S. F. Badylak and M. Modo, *Acta Biomater.*, 2017, **63**, 50–63.
3 S. K. Seidlits, Z. Z. Khaing, R. R. Petersen, J. D. Nickels, J. E. Vanscoy, J. B. Shear and C. E. Schmidt, *Biomaterials*, 2010, **31**, 3930–3940.
4 K. Hu, N. Zhou, Y. Li, S. Ma, Z. Guo, M. Cao, Q. Zhang, J. Sun, T. Zhang and N. Gu, *ACS Appl. Mater. Interfaces*, 2016, **8**, 15113–15119.
5 M. Jazayeri, M. A. Shokrgozar, N. Haghighipour, B. Bolouri, F. Mirahmadi and M. Farokhi, *Cell J.*, 2017, **19**, 34–44.
6 S. Mayer-Wagner, A. Passberger, B. Sievers, J. Aigner, B. Summer, T. S. Schiergens, V. Jansson and P. E. Müller, *Bioelectromagnetics*, 2011, **32**, 283–290.
7 R. J. Midura, M. O. Ibiwoye, K. A. Powell, Y. Sakai, T. Doehring, M. D. Grabiner, T. E. Patterson, M. Zborowski and A. Wolfman, *J. Orthop. Res.*, 2005, **23**, 1035–1046.
8 N. A. Walker, C. R. Denegar and J. Preische, *J. Athl. Train.*, 2007, **42**, 530–535.
9 H. Mahboudi, B. Kazemi, M. Soleimani, H. Hanaee-Ahvaz, H. Ghanbarian, M. Bandehpour, S. E. Enderami, M. Kehtari and G. Barati, *Gene*, 2018, **643**, 98–106.
10 Z. Chen, C. Yan, S. Yan, Q. Liu, M. Hou, Y. Xu and R. Guo, *Theranostics*, 2018, **8**, 1146–1158.
11 S. Majumdar, P. Pothirajan, D. Dorcemus, S. Nukavarapu and M. Kotecha, *Ann. Biomed. Eng.*, 2016, **44**, 1120–1127.
12 E. Mauri, E. Micotti, A. Rossetti, L. Melone, S. Papa, G. Azzolini, S. Rimondo, P. Veglianese, C. Punta, F. Rossi and A. Sacchetti, *Soft Matter*, 2018, **14**, 558–565.
13 Y. Xia, J. Sun, L. Zhao, F. Zhang, X. J. Liang, Y. Guo, M. D. Weir, M. A. Reynolds, N. Gu and H. H. K. Xu, *Biomaterials*, 2018, **183**, 151–170.
14 J. Zhuang, S. Lin, L. Dong, K. Cheng and W. Weng, *Acta Biomater.*, 2018, **71**, 49–60.
15 J. H. Huang, Y. J. Liang, Z. W. Huang, P. C. Zhao, Q. Liang, Y. L. Liu, L. Duan, W. Liu, F. Y. Zhu, L. M. Bian, J. Xia, J. Y. Xiong and D. P. Wang, *ACS Biomater. Sci. Eng.*, 2019, **5**, 2200–2207.
16 M. P. van den Borne, N. J. Raijmakers, J. Vanlauwe, J. Victor, S. N. de Jong, J. Bellemans and D. B. Saris, *Osteoarthr. Cartil.*, 2007, **15**, 1397–1402.
17 P. Mainil-Varlet, T. Aigner, M. Brittberg, P. Bullough, A. Hollander, E. Hunziker, R. Kandel, S. Nehrer, K. Pritzker, S. Roberts and E. Stauffer, *J. Bone Jt. Surg., Am. Vol.*, 2003, **85**, 45–57.
18 C. Hoemann, R. Kandel, S. Roberts, D. B. Saris, L. Creemers, P. Mainil-Varlet, S. Méthot, A. P. Hollander and M. D. Buschmann, *Cartilage*, 2011, **2**, 153–172.
19 A. D. Olubamiji, Z. Izadifar, J. L. Si, D. M. Cooper, B. F. Eames and D. X. Chen, *Biofabrication*, 2016, **8**, 025020.
20 E. B. Hunziker, *Osteoarthr. Cartil.*, 2002, **10**, 432–463.
21 J. E. Bekkers, L. B. Creemers, A. I. Tsuchida, M. H. van Rijen, R. J. Custers, W. J. Dhert and D. B. Saris, *Osteoarthr. Cartil.*, 2013, **21**, 950–956.
22 H. J. Li, C. Hu, H. J. Yu and C. Z. Chen, *RSC Adv.*, 2018, **8**, 3736–3749.
23 A. I. Caplan, *Tissue Eng.*, 2005, **11**, 1198–1211.
24 I. Sekiya, M. Ojima, S. Suzuki, M. Yamaga, M. Horie, H. Koga, K. Tsuji, K. Miyaguchi, S. Ogishima, H. Tanaka and T. Muneta, *J. Orthop. Res.*, 2012, **30**, 943–949.
25 E. A. Jones, A. English, K. Henshaw, S. E. Kinsey, A. F. Markham, P. Emery and D. McGonagle, *Arthritis Rheum.*, 2004, **50**, 817–827.
26 A. M. Alshehri, O. C. Wilson Jr, B. Dahal, J. Philip, X. Luo and C. B. Raub, *Colloids Surf., B*, 2017, **159**, 945–955.
27 Y. M. Lu, Y. W. Zhang and Y. X. Zhao, *Synthetic Technology & Application*, 2017, **32**, 1–6.
28 O. Im, J. Li, M. Wang, L. G. Zhang and M. Keidar, *Int. J. Nanomed.*, 2012, **7**, 2087–2099.
29 G. R. Mahdavinia, A. Mosallanezhad, M. Soleymani and M. Sabzi, *Int. J. Biol. Macromol.*, 2017, **97**, 209–217.
30 X. Y. Gong, F. L. Wang, Y. Huang, X. Lin, C. Chen, F. Y. Wang and L. Yang, *RSC Adv.*, 2018, **8**, 7633–7640.
31 S. Tang, K. Hu, J. Sun, Y. Li, Z. Guo, M. Liu, Q. Liu, F. Zhang and N. Gu, *ACS Appl. Mater. Interfaces*, 2017, **9**, 10446–10452.
32 X. Zheng, X. B. Wang and Y. X. Chen, *Chin. J. Orthop.*, 2015, **23**, 1104–1107.
33 H. Kavand, N. Haghighipour, B. Zeynali, E. Seyedjafari and B. Abdemami, *Artif. Organs*, 2016, **40**, 929–937.
34 D. Parate, A. Franco-Obregón, J. Fröhlich, C. Beyer, A. A. Abbas, T. Kamarul, J. H. P. Hui and Z. Yang, *Sci. Rep.*, 2017, **7**, 9421–9429.
35 T. Lu, Y. X. Huang, C. Zhang, M. X. Chai and J. Zhang, *Genet. Mol. Res.*, 2015, **14**, 11535–11542.
36 C. L. Ross, M. Siriwardane, G. Almeida-Porada, C. D. Porada, P. Brink, G. J. Christ and B. S. Harrison, *Stem Cell Res.*, 2015, **15**, 96–108.

